applied sciences

MDPI

*Article*

# A Comparative Performance Analysis of Four Wind Turbines with Counter-Rotating Electric Generators

**Mircea Neagoe [1], Radu Saulescu [2], Codruta Jaliu [1], Olimpiu Munteanu [1] and Nadia Cretescu [1,*]**

[1] Renewable Energy Systems and Recycling R&D Centre, Faculty of Product Design and Environment, Transilvania University of Brasov, 500036 Brasov, Romania; mneagoe@unitbv.ro (M.N.); cjaliu@unitbv.ro (C.J.); omunt@unitbv.ro (O.M.)

[2] Design of Mechanical Elements and Systems R&D Centre, Faculty of Product Design and Environment, Transilvania University of Brasov, 500036 Brasov, Romania; rsaulescu@unitbv.ro

* Correspondence: ncretescu@unitbv.ro; Tel.: +40-268-413-000

**Abstract:** Wind energy conversion systems play a major role in the transition to carbon-neutral power systems, and obviously, a special attention is paid in identifying the most effective solutions for a higher valorization of the local wind potential. In this context, this paper presents a comparative study on the energy performances of wind turbines (WTs) that include a counter-rotating electric generator. Starting from an innovative concept proposed by the authors for a reconfigurable wind turbine with three clutches, four cases of WTs with counter-rotating generators are studied: a system with three wind rotors (WRs) and a 2-DOF (degrees of freedom) planetary speed increaser (Case A), with two counter-rotating WRs and a 1-DOF (Case B) or a 2-DOF (Case C) speed increaser and a 1-DOF single rotor wind system (Case D). An analytical archetype model for angular speeds, torques, powers and efficiency of the reconfigurable planetary speed increaser, corresponding to the general case with three inputs (Case A), was firstly derived. The analytical models of the other three cases (B, C and D) were results by customizations of the archetype model according to the kinematic- and static-specific effects of engaging/disengaging the clutches. The simulation of the analytical models for a numerical representative example with two variable parameters (input speed ratio $k_\omega$ and input torque ratio $k_t$) allows highlighting the influence of various parameters (number of WRs, speed increaser DOF, $k_\omega$ and $k_t$) on the input powers, power that flows through the planetary transmission and mechanical power supplied to the electric generator, as well as on the transmission efficiency. The obtained results show that the output power increases with the increase of the number of wind rotors, the transmission efficiency is the maximum for $k_t = 1$ and the speed amplification ratio increases with the ratio $k_\omega$.

**Keywords:** renewable energy; wind turbine; wind rotor; counter-rotating electric generator; speed increaser; steady-state modeling; efficiency; power flow



**Citation:** Neagoe, M.; Saulescu, R.; Jaliu, C.; Munteanu, O.; Cretescu, N. A Comparative Performance Analysis of Four Wind Turbines with Counter-Rotating Electric Generators. *Appl. Sci.* **2022**, *12*, 4233. https://doi.org/10.3390/app12094233

Academic Editor: José A. F. O. Correia

Received: 12 March 2022
Accepted: 18 April 2022
Published: 22 April 2022



## 1. Introduction

The importance of replacing fossil fuel-based energy with clean energy in the concern for the sustainable development of human society is well-known, achieving green economic growth in the context of reducing its impact on climate change. Thus, the generation of electricity with renewable energy systems can reduce global greenhouse gas emissions to a large extent while reducing environmental pollution.

A significant share of clean electricity is obtained by converting wind kinetic energy by using wind turbines (WTs). In order to be accessible and feasible, wind turbines must meet several specific requirements, the conversion efficiency of wind energy into electricity being one of the most important technical issues. Therefore, it is necessary to optimize wind turbines by designing and developing efficient solutions; thus, the following main directions of scientific research have been identified in the literature:

- the design and development of novel solutions for wind turbines or their main components and an estimation of their performances;
- increasing the efficiency and/or energy performance of existing WTs;
- functional optimization of existing WT subsystems.

Special attention is also paid in the literature to the comparative study of various types of wind turbines: conventional (with a single wind rotor and electric generator with a fixed stator) and unconventional: dual- and multi-rotor WTs, with counter-rotating generators, with diverse types of speed increasers, etc.

The design of new or improved wind turbines is a constant concern of researchers and developers in the field. Thus, Oprina et al. [1] conducted a literature review of the main results on counter-rotating wind turbines (CRWTs) in terms of the design and methods for estimating their performances. Didan et al. [2] investigated experimentally the performance of a novel vertical axis counter-rotating wind turbine, and Pacholczyk et al. [3] analyzed a new small CRWT considering the influence of distance between the two wind rotors, its performance being highlighted using the computational fluid dynamics (CFD) method. An original small CRWT with a vertical shaft was proposed by West in a patent [4], in which the input motions of the two rotors are added by means of a gear transmission; a novel torque-adding CRWT was proposed by Neagoe et al. [5], considering also adding speed in the counter-rotating generator. Saulescu et al. presented in [6] an algorithm for the conceptual synthesis of systems with one or two counter-rotating wind rotors and with conventional or counter-rotating electric generators. Another way to increase the performances of wind turbines addressed the counter-rotating wind systems by implementing a counter-rotating double-sided flux switching permanent magnet generator, as proposed by Mirnikjoo et al. [7] and tested by Kutt [8]. A novel concept of CRWTs, including a 1-DOF (degree of freedom) planetary speed increaser with two inputs and one output, was proposed by Neagoe et al. in [9]. The design of multi-rotor and multi-generator WTs with a lattice tower was presented in [10]. Cho et al. [11] proposed, developed and experimentally tested an integrated control algorithm for a new dual-rotor wind turbine with a counter-rotating generator, designed to maximize the output power of the wind turbine. Jelaska et al. [12] proposed a wind system with two inputs and one output, one input being connected to a wind rotor and the other input to a motor aiming at maintaining a constant speed at the electric generator shaft. Unlike the previous studies, which refer to low- and medium-power systems, Qiu et al. [13] presented the main types of wind systems with one input and high output capacity. The performances of a CRWT with a conventional generator were analyzed by Saulescu et al. in [14] based on a steady-state operating point; the same authors approached in [15] the analysis of the efficiency of several speed increasers for systems with two inputs and one output with different mounting situations. Vasel-Be-Hagh et al. [16] analyzed the performance of a CRWT farm, and Blanco et al. investigated theoretically and experimentally the performance (power coefficient) of a vertical axis Savonius wind turbine integrating an innovative rotor with Fibonacci spiral geometry [17].

The performances of existing wind turbines have been studied by many researchers considering various indicators (capacity factor, availability, failure rate, downtime, power coefficient, efficiency, reliability, etc.) and using a wide range of data and methods, such as those systematized by Pfaffel et al. [18], the empirical mode decomposition method [19,20] or methods such as experiments and the Lattice Boltzmann model combined with Large Eddy Simulation [21] applied to a horizontal axis counter-rotating wind turbine. The performances of dual-rotor (co- and counter-rotating) wind turbines were highlighted also by Lam et al. in [22], ideas that were further developed by Lipian et al. [23] and Bani-Hani et al. [24]. The performance of a CRWT was discussed by Erturk et al. [25] in the case of implementing a counter-rotating generator, while Pamuji et al. compared rotary systems with two or three wind rotors [26]. Neagoe et al. analyzed in [27] the stationary operating point of a 2-DOF CRWT with a counter-rotating generator. Fan et al. [28] analyzed the influence of three-stage transmission vibrations on the performance of horizontal axis wind

systems operating in low-wind speed areas. Chaichana et al. studied in a wind tunnel the effect of the speed ratios of two counter-rotating rotors of a vertical axis wind turbine [29]; on the same CRWT type, Didane et al. [30] investigated the aerodynamic characteristics, power and torque coefficients. In [31], Didane et al. highlighted the performance of a CRWT with Darius H-type rotors using three-dimensional CFD models based on the K-omega Shear Stress Transport turbulence model; the same method was applied by Cao et al. [32] for a similar turbine on a floating platform. The performance of a horizontal axis CRWT with identical front and rear rotors was highlighted by Ilmunandar et al. in [33], while Koehuan et al. [34] analyzed the performance of the same wind turbine type by considering the ratio of wind rotor diameters as a dimensionless parameter.

The main WT subsystems addressed extensively by researchers are wind rotors, electric generators and speed increasers. Li et al. studied in [35] the effect of the number of blades on the aerodynamic forces of a vertical axis wind turbine, while the design of the WT blade shapes and their influence on the power coefficient in static and dynamic conditions were addressed in [36]. Mirnikjoo et al. investigated the performance of a counter-rotating electric generator [37].

Several representative speed reducers for which the power flow was reversed (and, hence, used as a speed increaser) were analyzed by Jaliu et al. in [38], while Saulescu et al. [39] proposed and modeled a speed increaser able to be operated with one input and one or two outputs. Other novel solutions of planetary speed increasers have been presented and analyzed in the literature: a 2-DOF hybrid transmission for variable speed wind turbines [12] and a two-input one-output cylindrical planetary gear set with satellites in a series [40]. The dynamic properties of a speed increaser and the steady-state operating point were highlighted by Herzog et al. [41] by studying the behavior of a wind turbine with counter-rotating rotors using a wind tunnel and the CFD method. Bharani et al. [42] classified the gearbox technologies for horizontal axis wind systems into three categories (planetary gearbox, continuous variable transmission and magnetic gearbox) and studied their performances based on indicators such as the torque output, tracking accuracy and durability. Qiu et al. summarized the gear mechanisms used in wind turbines [13]. Recent technologies and development trends of mechanical transmissions were systematized by Nejad et al. [43], and Concli et al. analyzed the behavior of the gear teeth using artificial neural networks [44] or the load capacity and its influence on the condition of the teeth [45]. The dynamic behavior of speed increasers was addressed by Wu et al. [46] by modeling the lateral-torsional coupling of the transmission of a large wind turbine. Lee et al. [47] proposed a testing rig, patented by the authors, used to investigate the mechanical power flow of a speed increaser into a high-speed wind turbine, while Lin et al. developed a new concept of a speed increaser with a parallel power flow implemented in a wind turbine with two inputs and one output [48].

Several studies have compared the efficiency of counter-rotating vs. conventional WTs, concluding that counter-rotating systems can generate up to 40% more electricity. Thus, Climescu et al. [49] analyzed the dynamics of counter-rotating vs. conventional wind systems with a cylindrical gearbox. Saulescu et al. approached comparatively the stationary operating point for wind turbines with two counter-rotating rotors vs. one rotor and 1-DOF vs. 2-DOF speed increasers [50], wind systems with one rotor and counter-rotating vs. traditional (with fixed stator) electric generator [51] and wind systems with two counter-rotating rotors and counter-rotating vs. a traditional generator [52]. Farahani et al. [53] showed comparatively the dynamic behavior of a CRWT in several operating situations.

Considering the variability of wind speed during the year, the optimization of wind energy harvesting and the transformation as efficient as possible into electricity are major challenges for research in the field. Dual- or multi-rotor wind turbines with counter-rotating generators are a promising recent technology still insufficiently explored for large-scale development and implementation. This research is also part of this knowledge development effort by proposing a comparative analysis of the energy performance of four wind turbines with a counter-rotating electric generator that integrate a planetary speed increaser with an

innovative variable structure patented by the authors. This transmission allows the wind turbine to operate with one, two or three counter-rotating WRs by means of three clutches.

The manuscript is organized as follows: Section 2 is devoted to problem formulation and presents the four studied configurations (cases) of the WTs with a counter-rotating generator. Section 3 details the analytical modeling method and presents the kinematic, static, power and efficiency results in the four cases derived from a general model. For a representative numerical set, Section 4 presents the simulation results and discussions on the analyzed WT performances. The final conclusions of the paper are drawn in Section 5.

## 2. Problem Formulation

The wind systems with counter-rotating generators (*WSCGs*) have superior conversion efficiencies compared to conventional generators (with fixed stator) due to the branched transmission of mechanical power and higher relative speed between the rotor (GR) and the stator (GS) of the electric generator (G). A counter-rotating generator has both armatures (GR and GS) movable and rotates in opposite directions; usually, due to inertial reasons, the generator rotor has a higher speed than the stator. However, the energy performance of *WSCGs* is significantly influenced by the number of WRs, as well as by the speed increaser type. In order to highlight the influence of the number of WRs (inputs) and of the structural degree of freedom, a comparison between *WSCGs* with 1-DOF or 2-DOF speed increasers with one input (i.e., with one *WR* and the total number of external connections $L = 3$, implicitly), two inputs (two *WRs* and $L = 4$) and three inputs (three *WRs* and $L = 5$) is further approached. To this end, a planetary transmission with a variable structure, based on three clutches and derived from a solution for which the authors have a patent application [54], is proposed; by appropriate combinations of clutch engaging and disengaging, the transmission can operate in various structures, of which four cases were selected (Figure 1):

- Case A: 2-DOF (differential) transmission with three inputs (2-DOF, $L = 5$, and three *WRs*);
- Case B: 1-DOF (monomobile) transmission with two inputs (1-DOF, $L = 4$, and two *WRs*);
- Case C: 2-DOF transmission with two inputs (2-DOF, $L = 4$, and two *WRs*);
- Case D: 1-DOF transmission with one input (1-DOF, $L = 3$, and one *WR*).

As a result, the energy performances of *WSCG*s with two or three wind rotors can be directly compared with those of conventional wind turbines (with one wind rotor), highlighting the specific differences of cases with 1-DOF vs. 2-DOF transmissions.

The approach starts from a "variable" structure, based on setting the clutches C1 ... C3 (Figure 1); this structure contains: three wind rotors (a permanent primary rotor $R1$ and two secondary rotors $R2$ and $R3$ activated by clutches C2 and C3, respectively), a planetary gear set with bevel gears I $\equiv$ 2-1″-1′-3-$H_1$ (equipped with clutch C1 for blocking the satellite carrier $H_1$) and a differential cylindrical planetary gear set II $\equiv$ 4-5-6-$H_2$ with two counter-rotating outputs, 6 and 7, secured to the rotor *GR* and the stator *GS*, respectively.

The primary rotor $R1$ is coupled to the bevel gear (2), which is assembled on the carrier $H_2$. The power generated by $R1$ is distributed on two branches to the planetary gear set II through the bevel sun gear (3), assembled into the ring sun gear (4) and directly to the carrier $H_2$; further, the power is transmitted by gear set II to the rotor $GR \equiv 6$ and stator $GS \equiv 7$, respectively.

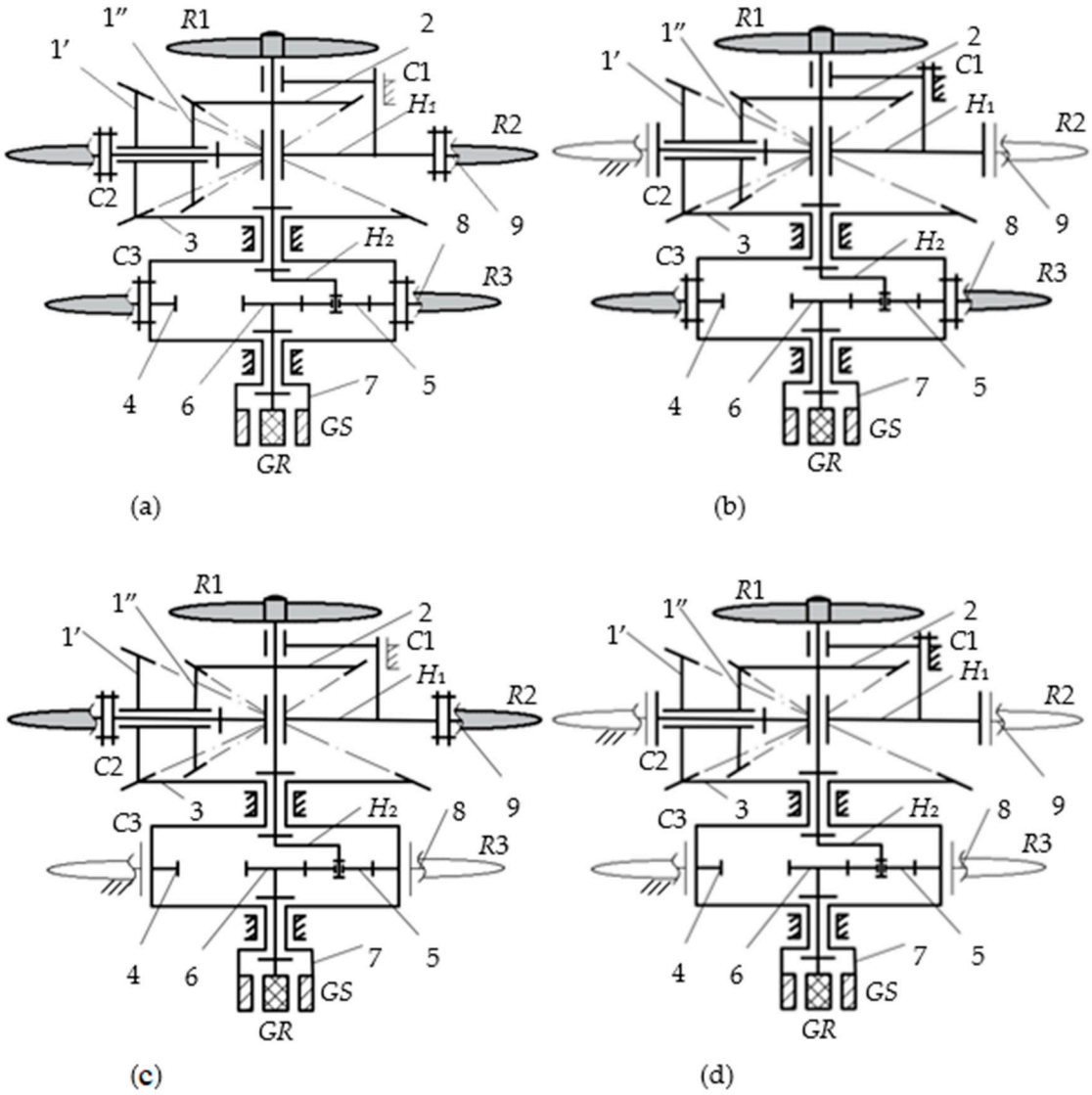


**Figure 1.** Schemes of the *WSCGs* with a "variable" structure: (**a**) *C*1 = 0, *C*2 = *C*3 = 1: Case A (2-DOF, L = 5); (**b**) *C*1 = *C*3 = 1, *C*2 = 0: Case B (1-DOF, L = 4); (**c**) *C*1 = *C*3 = 0, *C*2 = 1: Case C (2-DOF, *L* = 4); (**d**) *C*1 = 1, *C*2 = *C*3 = 0: Case D (1-DOF, *L* = 3).

Denoting a disengaged clutch by *Ci* = 0 and an engaged clutch by *Ci* = 1 (*i* = 1, 2, 3), the structures related to Cases A, B, C and D can be described as follows:

- Case A, Figure 1a: *C*1 = 0, *C*2 = *C*3 = 1, 2-DOF transmission with three inputs and two outputs (*L* = 5);
- Case B, Figure 1b: *C*1 = *C*3 = 1, *C*2 = 0, 1-DOF transmission with two inputs and two outputs (*L* = 4); for *C*1 = 1, the bevel transmission I is a 1-DOF gear set with fixed axes, and, for *C*2 = 0, the rotor *R*2 idles and torque $T_{R2} = 0$, implicitly. In order to facilitate the kinematic modeling, it is considered that the clutch disengaging, afferent to a rotor *R*, is accompanied by fixing the rotor to the base, i.e., the rotational speed $\omega_R = 0$;
- Case C, Figure 1c: *C*1 = *C*3 = 0, *C*2 = 1, 2-DOF transmission with two inputs and two outputs (*L* = 4); analogous to Case B, for *C*3 = 0, the rotor *R*3 becomes inactive and blocked, i.e., $T_{R3} = 0$ and $\omega_{R3} = 0$;
- Case D, Figure 1d: *C*1 = 1, *C*2 = *C*3 = 0, 1-DOF transmission with one input and two outputs (*L* = 3); analogous with Cases B and C, the rotors *R*2 and *R*3 become

inactive and blocked for $C2 = C3 = 0$, i.e., $T_{R2} = 0$, $\omega_{R2} = 0$ and $T_{R3} = 0$, $\omega_{R3} = 0$, respectively.

The four variants of *WSCGs* (Figure 1) use the same speed increaser under the following premises:

- homologous gears of the four *WSCGs* have the same number of teeth $z_i$, $i = 1', 1'', \ldots, 6$;
- homologous gear pairs with fixed axes have the same efficiency;
- the three wind rotors have the possibility to modify the pitch angle of their blades to adjust the input powers, the angular speeds and the input torques implicitly while considering a constant wind speed (i.e., a steady-state regime);
- in order to facilitate the kinematic modeling, it is considered that the clutch disengaging for a wind rotor is accompanied by the rotor locking at the base, which means that both the rotor torque and speed become null.

Under these premises, the problem addressed in the paper refers to the analytical modeling of the parameters considered as the main comparison criteria: the kinematic amplification ratio of the speed from the primary rotor $R1$ to the generator $G$ $(i_a)$, the transmission efficiency $(\eta)$ and the mechanical power transmitted to the electric generator $(P_G)$, as well as the power flow. For simplicity, the meaning of the symbols used in the equations is detailed in the Nomenclature section, without repeating it in the text.

## 3. Closed-Form Modeling

The kinematic and static models of the *WSCGs* illustrated in Figure 1 can be derived based on the block diagrams from Figure 2. The following correlations [55] can be written by decomposing the complex transmissions into gear sets I and II, according to the block diagrams in Figure 2:

- Planetary gear set I:

$$\text{I}: \begin{cases} i_{32}^{H_1} = i_{01} = \frac{\omega_{3H_1}}{\omega_{2H_1}} = -\frac{z_{1'}}{z_3}\frac{z_2}{z_{1''}} \\ \omega_3 = \omega_2 i_{01} - \omega_{H_1}(1 - i_{01}) \;\Rightarrow\; i_{32} = i_{01} + \frac{\omega_{H_1}}{\omega_2}(1 - i_{01}) \\ T_3 i_{01} \eta_{01}^{x} + T_{2'} = 0 \\ T_3 + T_{2'} + T_{H_1} = 0 \end{cases} \tag{1}$$

where $x = \pm 1$, depending on the direction of the power flow transmission through the fixed axis mechanisms associated with the planetary gear set, obtained by reversing the motion with respect to $H_1$ [55]. For Case A (Figure 1a) and Case B (Figure 1b), the sign of $x$ depends on the ratio $k_t = -T_{R3}/T_{R1}$: for $k_t > 1$, $x = +1$, and for $k_t < 1$, $x = -1$. For Cases C (Figure 1c) and D (Figure 1d), $x = -1$.

- Planetary gear set II:

$$\text{II}: \begin{cases} i_{64}^{H_2} = i_{02} = \frac{\omega_{6H_2}}{\omega_{4H_2}} = -\frac{z_4}{z_6} \\ \omega_6 = \omega_4 i_{02} + \omega_{H2}(1 - i_{02}) \;\Rightarrow\; i_{64} = i_{02} + \frac{\omega_{H_2}}{\omega_4}(1 - i_{02}) \\ T_6 i_{02} \eta_{02}^{w} + T_4 = 0 \\ T_6 + T_4 + T_{H_2} = 0 \end{cases} \tag{2}$$

where the sign of the exponent $w$ is obtained as follows [55]:

$$w = \operatorname{sgn}(\omega_{6H_2} T_6) = \operatorname{sgn}\left(\frac{i_{02}}{1 - i_{02}}\right) = -1 \tag{3}$$

where sgn is the signum function.

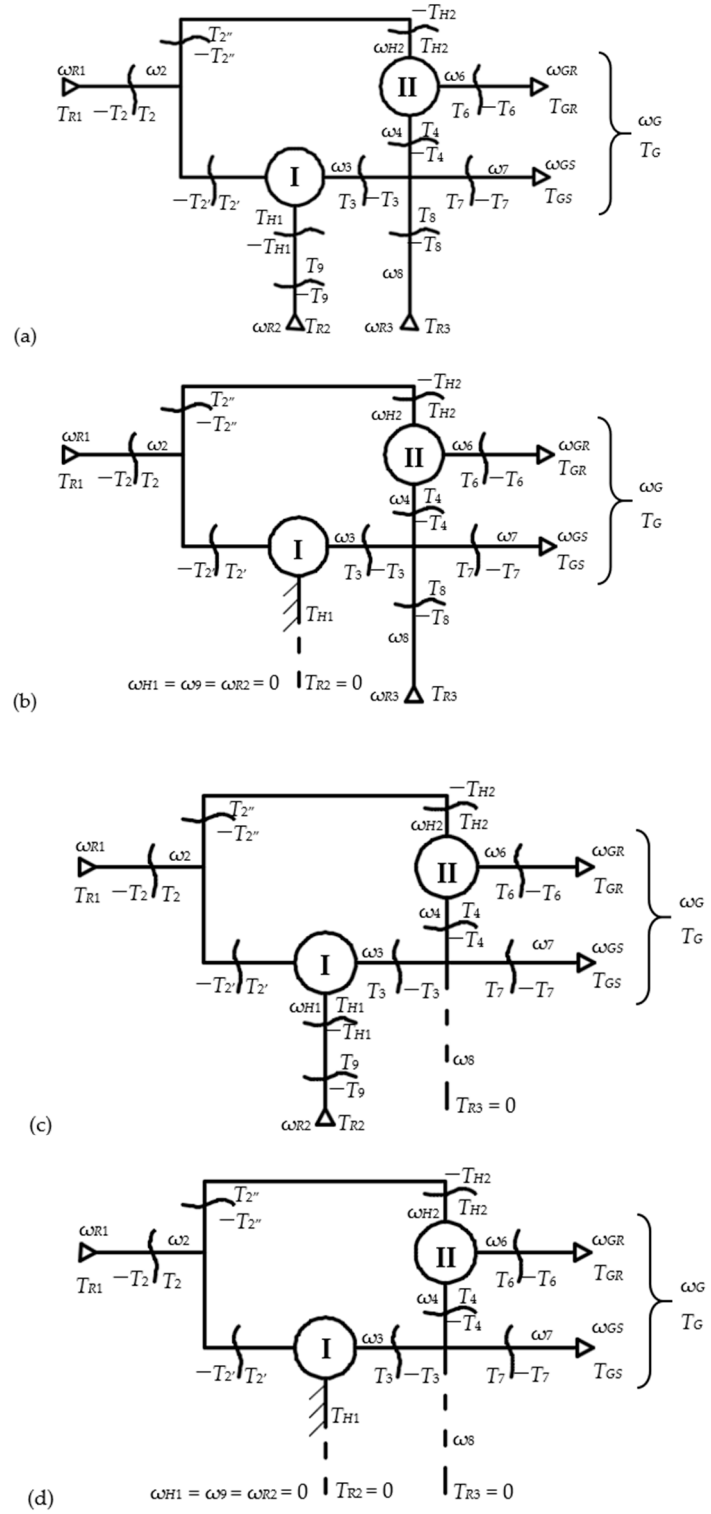


**Figure 2.** Block diagrams of the transmissions from Figure 1: (**a**) Case A (Figure 1a); (**b**) Case B (Figure 1b); (**c**) Case C (Figure 1c); (**d**) Case D (Figure 1d).

The kinematic and static modeling in the general case (Case A) is further presented considering Equations (1) and (2), to which the kinematic and static correlations related to the connections between the planetary gear sets, the wind rotors and the electric generator are added. The relations for the other three functional cases (B, C and D) are obtained by customizing the analytical archetype model obtained in Case A.

### 3.1. Kinematic Modeling

The transmission with three inputs (Case A, Figure 1a) is characterized by two independent external speeds; for instance, $\omega_{R1}$ and $\omega_{R2}$. For simplicity, it is preferable to use the input speed ratio $k_\omega = -\omega_{R2}/\omega_{R1}$ as an independent variable instead of the speed $\omega_{R2}$. According to Figure 2a, the following correlations related to the connections between the *WSCG* components can be added to the kinematic equations in Systems (1) and (2):

$$\begin{cases} \omega_{R1} = \omega_2 = \omega_{H_2} \\ \omega_{R2} = \omega_9; \;\; \omega_{R2} = -k_\omega \omega_{R1} \\ \omega_9 = \omega_{H_1} \\ \omega_3 = \omega_4 = \omega_7 = \omega_8 \\ \omega_7 = \omega_{GS}; \;\; \omega_8 = \omega_{R3} \\ \omega_6 = \omega_{GR} \\ \omega_G = \omega_{GR} - \omega_{GS} \end{cases} \tag{4}$$

The obtained set of 14 independent equations with 16 unknown parameters allows the description of the 14 dependent kinematic variables ($\omega_{R2}$, $\omega_{R3}$, $\omega_{GR}$, $\omega_{GS}$, $\omega_G$, $\omega_2$, $\omega_3$, $\omega_4$, $\omega_6$, $\omega_7$, $\omega_8$, $\omega_9$, $\omega_{H_1}$ and $\omega_{H_2}$), depending on the independent variables $\omega_{R1}$ and $k_\omega$.

The other three cases (B, C and D) can be modeled kinematically based on the relations previously obtained for the archetype model, in which the following particularizations occur:

- Case B: $C1 = 1$, $C2 = 0$ and $\omega_{R2} = 0$; implicitly: $\omega_9 = \omega_{H1} = 0$ (Figure 2b);
- Case C: $C3 = 0$ and $\omega_{R3} = 0$; implicitly: $\omega_8 = 0$ and $\omega_7 = \omega_4 = \omega_3$ $(\neq 0)$ (Figure 2c);
- Case D: $C1 = 1$, $C2 = C3 = 0$ and $\omega_{R2} = 0 = \omega_{R3} = 0$; implicitly: $\omega_9 = \omega_{H1} = 0$, $\omega_8 = 0$ and $\omega_7 = \omega_4 = \omega_3$ $(\neq 0)$ (Figure 2d).

The transmission amplification ratio $i_a$ can be obtained with the relation:

$$i_a = \frac{\omega_G}{\omega_{R1}} \tag{5}$$

The kinematic correlations of the speed increasers from Figure 1, systematized in Table 1, can be obtained by solving the set of kinematic Equations (1), (2), (4) and (5) and considering the previous particularizations. It can be observed that, except for the speed $\omega_{R3}$, the relations are identical for Cases A and C (2-DOF variants) and B and D (1-DOF variants), respectively.

**Table 1.** The analytical expressions of the dependent kinematic parameters and the amplification kinematic ratio corresponding to the four cases (Figures 1 and 2).

| | **Case A** | **Case C** | **Case B** | **Case D** |
|---|---|---|---|---|
| $\omega_{R2}$ | $-\omega_{R1}k_\omega$ | $-\omega_{R1}k_\omega$ | 0 | 0 |
| $\omega_{R3}$ | $\omega_{R1}[i_{01} - k_\omega(1 - i_{01})]$ | 0 | $\omega_{R1}i_{01}$ | 0 |
| $\omega_{GR}$ | $\omega_{R1}[i_{02}(i_{01} - 1)(1 + k_\omega) + 1]$ | | $\omega_{R1}[i_{02}(i_{01} - 1) + 1]$ | |
| $\omega_{GS}$ | $\omega_{R1}[i_{01} - k_\omega(1 - i_{01})]$ | | $\omega_{R1}i_{01}$ | |
| $\omega_G$ | $\omega_{R1}(1 - i_{01})(1 - i_{02})(1 + k_\omega)$ | | $\omega_{R1}(1 - i_{01})(1 - i_{02})$ | |
| $i_a$ | $(1 - i_{01})(1 - i_{02})(1 + k_\omega)$ | | $(1 - i_{01})(1 - i_{02})$ | |

### 3.2. Torque Modeling in the Steady-State Regime

The following set of static equations in steady-state conditions is obtained based on the torque equations that come from the modeling of the two planetary gear sets, according

to Equations (1) and (2), and the equations of static equilibrium for the shafts isolated from the *WSCG*—Case A (Figure 2a):

$$\begin{cases} T_{R1} - T_2 = 0 \\ T_2 - T_{2'} - T_{2''} = 0;\ T_{2'} = -\overline{i_{01}} T_3;\ T_{2''} = T_{H_2} \\ -T_3 - T_4 + T_7 + T_8 = 0 \\ T_9 - T_{H_1} = 0;\ T_{H_1} = \left(\overline{i_{01}} - 1\right) T_3;\ T_{H_2} = \left(\overline{i_{02}} - 1\right) T_6 \\ T_4 = -\overline{i_{02}} T_6 \\ T_{R2} - T_9 = 0;\ T_{R3} - T_8 = 0;\ T_{R3} = -k_t T_{R1} \\ T_{GR} - T_6 = 0;\ T_{GS} - T_7 = 0;\ T_G = T_{GR} = -T_{GS} \end{cases} \quad (6)$$

where $\overline{i_{01}} = i_{01}\eta_{01}^{x}$, $\overline{i_{02}} = i_{02}\eta_{02}^{w}$. Thus, a system of 16 linear equations with 16 dependent torques ($T_{R2}$, $T_{R3}$, $T_{GR}$, $T_{GS}$, $T_G$, $T_2$, $T_{2'}$, $T_{2''}$, $T_3$, $T_4$, $T_6$, $T_7$, $T_8$, $T_9$, $T_{H_1}$ and $T_{H_2}$) and two independent variables $T_{R1}$ and $T_{R3}$, replaced by $T_{R1}$ and the input torques ratio $k_t = -T_{R3}/T_{R1}$, is obtained. Relations (6) are valid for the other three cases by considering the following customizations:

- Case B: *C*2 = 0, $T_{R2} = 0$, and implicitly, $T_9 = 0$ and $T_{H_1} \neq 0$ (Figure 2b);
- Case C: *C*3 = 0, $T_{R3} = 0$, and implicitly, $T_8 = 0$ (Figure 2c);
- Case D: *C*2 = *C*3 = 0, $T_{R2} = 0$ and $T_{R3} = 0$, and implicitly, $T_8 = 0$, $T_9 = 0$ and $T_{H_1} \neq 0$ (Figure 2d).

Solving linear system (6), by taking into account the particularities of each case, leads to the torque expressions systematized in Table 2. It can be noticed that the torques in Table 2 have identical expressions in Cases A and B and C and D, respectively, except for the zero input torques; in addition, the torque relations for Cases C and D are obtained through the customization of Cases A and B by considering $k_t = 0$.

**Table 2.** Expressions of *WSCG* torques related to the four cases (Figures 1 and 2).

| | **Case A** | **Case B** | **Case C** | **Case D** |
|---|---|---|---|---|
| $T_{R2}$ | $T_{R1}(k_t - 1)$ | 0 | $-T_{R1}$ | 0 |
| $T_{R3}$ | $-T_{R1}k_t$ | | 0 | 0 |
| $T_{GR}$ | $-T_{R1}\frac{\left(1-k_t\overline{i_{01}}\right)}{\left(\overline{i_{01}}-1\right)\left(\overline{i_{02}}-1\right)}$ | | $-T_{R1}\frac{1}{\left(\overline{i_{01}}-1\right)\left(\overline{i_{02}}-1\right)}$ | |
| $T_{GS}$ | $T_{R1}\frac{\left(1-k_t\overline{i_{01}}\right)}{\left(\overline{i_{01}}-1\right)\left(\overline{i_{02}}-1\right)}$ | | $T_{R1}\frac{1}{\left(\overline{i_{01}}-1\right)\left(\overline{i_{02}}-1\right)}$ | |
| $T_{2'}$ | $-T_{R1}\frac{\overline{i_{01}}(k_t-1)}{\overline{i_{01}}-1}$ | | $T_{R1}\frac{\overline{i_{01}}}{\overline{i_{01}}-1}$ | |
| $T_{2''}$ | $-T_{R1}\frac{1-k_t\overline{i_{01}}}{\overline{i_{01}}-1}$ | | $-T_{R1}\frac{1}{\overline{i_{01}}-1}$ | |
| $T_3$ | $T_{R1}\frac{k_t-1}{\overline{i_{01}}-1}$ | | $-T_{R1}\frac{1}{\overline{i_{01}}-1}$ | |
| $T_4$ | $T_{R1}\frac{\overline{i_{02}}\left(1-k_t\overline{i_{01}}\right)}{\left(\overline{i_{01}}-1\right)\left(\overline{i_{02}}-1\right)}$ | | $T_{R1}\frac{\overline{i_{02}}}{\left(\overline{i_{01}}-1\right)\left(\overline{i_{02}}-1\right)}$ | |
| $T_{H_1}$ | $T_{R1}(k_t - 1)$ | | $-T_{R1}$ | |

Notes: $T_2 = T_{R1}$, $T_G = T_{GR}$, $T_6 = T_{GR}$, $T_7 = T_{GS}$, $T_8 = T_{R3}$, $T_9 = T_{R2}$ and $T_{H_2} = T_{2''}$.

### *3.3. Power and Efficiency Modeling in Steady-State Regime*

The mechanical power on the speed increaser shafts can be analytically determined by taking into account the kinematic results from Table 1 and the static ones from Table 2, depending on the independent parameters $T_{R1}$, $\omega_{R1}$, $k_t$ and $k_\omega$. The obtained power relations (i.e., the power $P_i = T_i \cdot \omega_i$ on the $i$ shaft, $i$ = 1, 2, ... ) are systematized in Table 3 for the four studied cases.

**Table 3.** *WSCG* power and efficiency expressions for the four cases (Figures 1 and 2).

| | **Case A** | **Case B** | **Case C** | **Case D** |
|---|---|---|---|---|
| $P_{R2}$ | $-\omega_{R1}T_{R1}k_\omega(k_t-1)$ | $0$ | $-\omega_{R1}T_{R1}k_\omega$ | $0$ |
| $P_{R3}$ | $-\omega_{R1}T_{R1}k_t[i_{01}-k_\omega(1-i_{01})]$ | $-\omega_{R1}T_{R1}k_t i_{01}$ | $0$ | $0$ |
| $P_{GR}$ | $-\omega_{R1}T_{R1}\frac{(1-k_t\overline{i_{01}})[i_{02}(i_{01}-1)(1+k_\omega)+1]}{(\overline{i_{01}}-1)(\overline{i_{02}}-1)}$ | $-\omega_{R1}T_{R1}\frac{(1-k_t\overline{i_{01}})[i_{02}(i_{01}-1)+1]}{(\overline{i_{01}}-1)(\overline{i_{02}}-1)}$ | $-\omega_{R1}T_{R1}\frac{i_{02}(i_{01}-1)(1+k_\omega)+1}{(\overline{i_{01}}-1)(\overline{i_{02}}-1)}$ | $-\omega_{R1}T_{R1}\frac{i_{02}(i_{01}-1)+1}{(\overline{i_{01}}-1)(\overline{i_{02}}-1)}$ |
| $P_{GS}$ | $\omega_{R1}T_{R1}\frac{(1-k_t\overline{i_{01}})[i_{01}-k_\omega(1-i_{01})]}{(\overline{i_{01}}-1)(\overline{i_{02}}-1)}$ | $\omega_{R1}T_{R1}\frac{i_{01}(1-k_t\overline{i_{01}})}{(\overline{i_{01}}-1)(\overline{i_{02}}-1)}$ | $\omega_{R1}T_{R1}\frac{i_{01}-k_\omega(1-i_{01})}{(\overline{i_{01}}-1)(\overline{i_{02}}-1)}$ | $\omega_{R1}T_{R1}\frac{i_{01}}{(\overline{i_{01}}-1)(\overline{i_{02}}-1)}$ |
| $P_G$ | $-\omega_{R1}T_{R1}\frac{(1-i_{01})(1-i_{02})(1+k_\omega)(1-k_t\overline{i_{01}})}{(\overline{i_{01}}-1)(\overline{i_{02}}-1)}$ | $-\omega_{R1}T_{R1}\frac{(1-i_{01})(1-i_{02})(1-k_t\overline{i_{01}})}{(\overline{i_{01}}-1)(\overline{i_{02}}-1)}$ | $-\omega_{R1}T_{R1}\frac{(1-i_{01})(1-i_{02})(1+k_\omega)}{(\overline{i_{01}}-1)(\overline{i_{02}}-1)}$ | $-\omega_{R1}T_{R1}\frac{(1-i_{01})(1-i_{02})}{(\overline{i_{01}}-1)(\overline{i_{02}}-1)}$ |
| $P_2$ | $T_{R1}\omega_{R1}$ | $T_{R1}\omega_{R1}$ | $T_{R1}\omega_{R1}$ | $T_{R1}\omega_{R1}$ |
| $P_{2'}$ | $-\omega_{R1}T_{R1}\frac{\overline{i_{01}}(k_t-1)}{\overline{i_{01}}-1}$ | $-\omega_{R1}T_{R1}\frac{\overline{i_{01}}(k_t-1)}{\overline{i_{01}}-1}$ | $\omega_{R1}T_{R1}\frac{\overline{i_{01}}}{\overline{i_{01}}-1}$ | $\omega_{R1}T_{R1}\frac{\overline{i_{01}}}{\overline{i_{01}}-1}$ |
| $P_{2''}$ | $-\omega_{R1}T_{R1}\frac{1-k_t\overline{i_{01}}}{\overline{i_{01}}-1}$ | $-\omega_{R1}T_{R1}\frac{1-k_t\overline{i_{01}}}{\overline{i_{01}}-1}$ | $-\omega_{R1}T_{R1}\frac{1}{\overline{i_{01}}-1}$ | $-\omega_{R1}T_{R1}\frac{1}{\overline{i_{01}}-1}$ |
| $P_3$ | $\omega_{R1}T_{R1}\frac{[i_{01}-k_\omega(1-i_{01})](k_t-1)}{\overline{i_{01}}-1}$ | $\omega_{R1}T_{R1}\frac{i_{01}(k_t-1)}{\overline{i_{01}}-1}$ | $-\omega_{R1}T_{R1}\frac{i_{01}-k_\omega(1-i_{01})}{\overline{i_{01}}-1}$ | $-\omega_{R1}T_{R1}\frac{i_{01}}{\overline{i_{01}}-1}$ |
| $P_4$ | $\omega_{R1}T_{R1}\frac{\overline{i_{02}}(1-k_t\overline{i_{01}})[i_{01}-k_\omega(1-i_{01})]}{(\overline{i_{01}}-1)(\overline{i_{02}}-1)}$ | $\omega_{R1}T_{R1}\frac{i_{01}\overline{i_{02}}(1-k_t\overline{i_{01}})}{(\overline{i_{01}}-1)(\overline{i_{02}}-1)}$ | $\omega_{R1}T_{R1}\frac{\overline{i_{02}}[i_{01}-k_\omega(1-i_{01})]}{(\overline{i_{01}}-1)(\overline{i_{02}}-1)}$ | $\omega_{R1}T_{R1}\frac{i_{01}\overline{i_{02}}}{(\overline{i_{01}}-1)(\overline{i_{02}}-1)}$ |
| $\eta$ | $\frac{(i_{01}-1)(i_{02}-1)(1-k_t\overline{i_{01}})}{(\overline{i_{01}}-1)(\overline{i_{02}}-1)(1-k_t i_{01})}$ | | $\frac{(i_{01}-1)(i_{02}-1)}{(\overline{i_{01}}-1)(\overline{i_{02}}-1)}$ | |

Notes: $P_2 = P_{R1}$, $P_6 = P_{GR}$, $P_7 = P_{GS}$, $P_8 = P_{R3}$, $P_9 = P_{R2}$, $P_{H_1} = P_{R2}$ and $P_{H_2} = P_{2''}$.

Starting from the efficiency expression in Case A, in the hypothesis of wind rotors operating as motors (i.e., $P_{Ri} > 0$, $i = 1, 2, 3$):

$$\eta = -\frac{P_G}{P_{R1} + P_{R2} + P_{R3}} = -\frac{\omega_{GR} T_{GR} + \omega_{GS} T_{GS}}{\omega_{R1} T_{R1} + \omega_{R2} T_{R2} + \omega_{R3} T_{R3}} \quad (7)$$

the efficiencies of the other speed increasers (Cases B, C and D) are obtained by customization; the analytical relations for the efficiency in the four cases are also systematized in Table 3.

## 4. Numerical Simulations and Discussions

The *WSCG* analytical model, described by the relations in Tables 1–3, contains eight independent parameters: the interior kinematic ratios $i_{01}$ and $i_{02}$, the interior efficiencies $\eta_{01}$ and $\eta_{02}$, the primary wind rotor power parameters ($\omega_{R1}$ and $T_{R1}$) and the ratios $k_\omega$ and $k_t$. The numerical simulations are based on the input data from Table 4, where $i_{01}$, $i_{02}$, $\eta_{01}$ and $\eta_{02}$ are constant parameters of the mechanical transmission, $k_\omega$ and $k_t$ are independent parameters used as variable simulation ratios whose values can be controlled by appropriately adjusting the pitch angles of the wind rotor blades.

**Table 4.** Input data for the numerical simulations of the analytical model.

| Planetary Gear Set | $i_0$ | $\eta_0$ | $k_\omega = -\frac{\omega_{R2}}{\omega_{R1}}$ | $k_t = -\frac{T_{R3}}{T_{R1}}$ |
|---|---|---|---|---|
| I | −1.5 | 0.8836 (=$0.94^2$) | −0.5 … 1 | - |
| II | −5 | 0.925 (=$0.95^2$) | - | 0 … 1.5 |

The numerical simulations are performed under the following assumptions:

- Both secondary rotors (*R*2 and *R*3) rotate in opposite directions to the primary rotor *R*1 (by exception, rotor *R*2 may also have the rotation direction of rotor *R*1, a situation highlighted in Section 4.1);
- The powers of rotors *R*1, *R*2 and *R*3 are input powers for the transmission, i.e., $P_{R1} > 0$, $P_{R2} > 0$ and $P_{R3} > 0$ (but there are also exceptions in which rotor *R*2 becomes the brake, i.e., $P_{R2} < 0$, as highlighted in Section 4.2);
- The counter-rotating electric generator *G* is characterized by the operating speed $\omega_G = \omega_{GR} - \omega_{GS}$, the torque $T_G = T_{GR} = -T_{GS}$ and by the mechanical power $P_G = T_G \omega_G$ (considered as the transmission output power, i.e., $P_G = T_G \omega_G < 0$, Figure 2);
- In order to simplify the comparative energy analysis of the selected cases, the mechanical characteristics related to the wind rotors and the generator are disregarded; as a result, the power of the primary rotor *R*1 will be further considered as the reference power, and the other powers will be expressed by ratios of the type $P_x / P_{R1}$, whatever the *x* shaft, called reduced powers (at the primary rotor).

### *4.1. Transmission Input Powers and Efficiency*

The analysis of the diagrams depicted in Figures 3–6 allows the following particularities to emerge:

(a) The ratios $k_\omega$ and $k_t$ directly influence the operation state of the secondary wind rotors *R*2 and *R*3 and the mechanical power flow through the planetary transmission implicitly; thus, for Case A, the variation ranges of these ratios for which the wind system operation makes sense are further analyzed, i.e., the secondary wind rotors *R*2 and *R*3 are motor sources ($P_{R2} > 0$ and $P_{R3} > 0$).

(b) In the premise $P_{R1} > 0$, the angular speed and the torque of the rotor *R*2 (controlled by $k_\omega$ and $k_t$) also influence the power of the secondary wind rotor *R*3 (Figures 3 and 4).

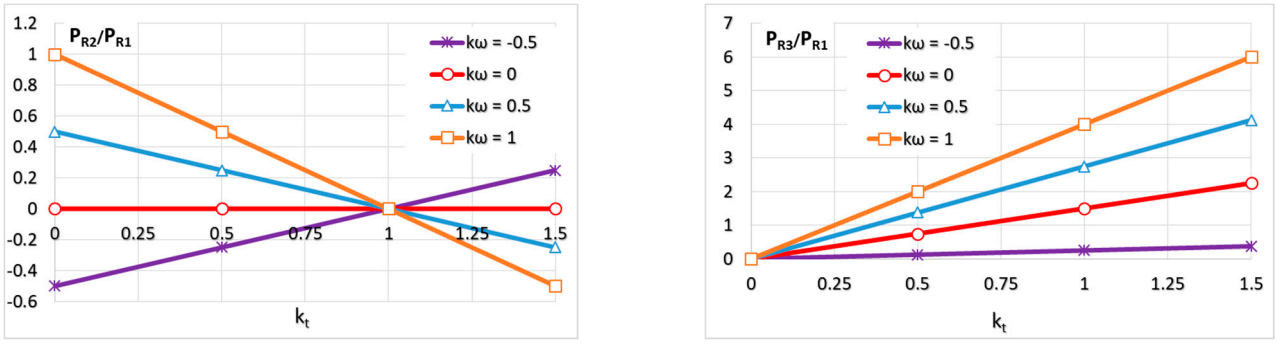


(**a**) (**b**)

**Figure 3.** Reduced input power variations depending on the ratio $k_t$ for various values of ratio $k_\omega$: (**a**) reduced power of the wind rotor R2; (**b**) reduced power of the wind rotor R3 (Case A).

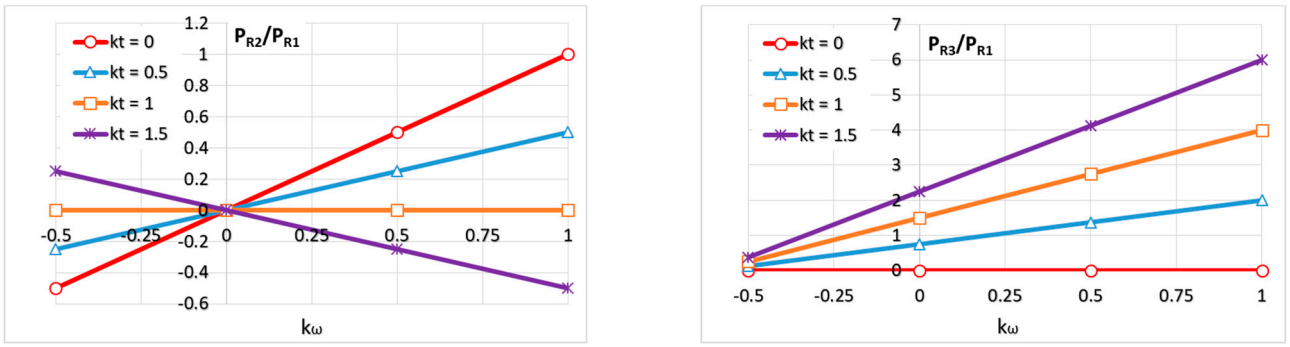


(**a**) (**b**)

**Figure 4.** Reduced input power variations depending on the ratio $k_\omega$ for various values of ratio $k_t$: (**a**) reduced power of the wind rotor R2; (**b**) reduced power of the wind rotor R3 (Case A).

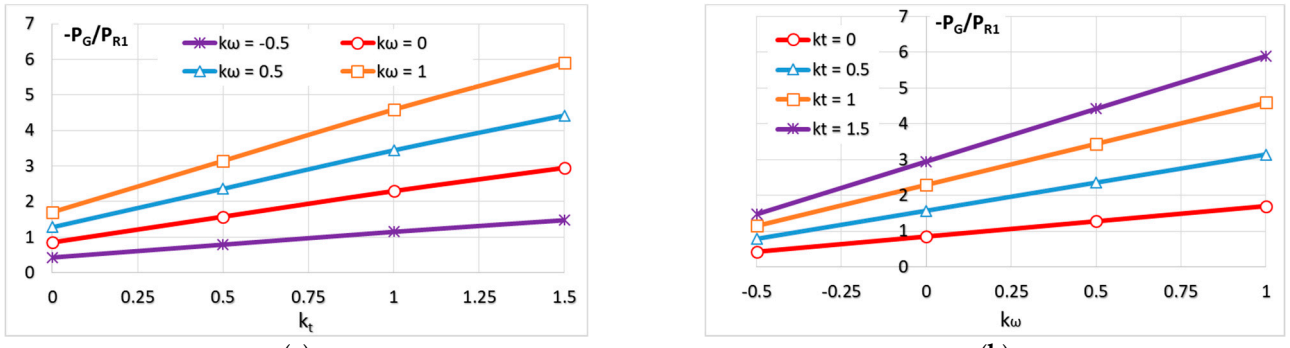


(**a**) (**b**)

**Figure 5.** Variations of the electric generator reduced power, depending on: (**a**) the ratio $k_t$; (**b**) the ratio $k_\omega$ (Case A).

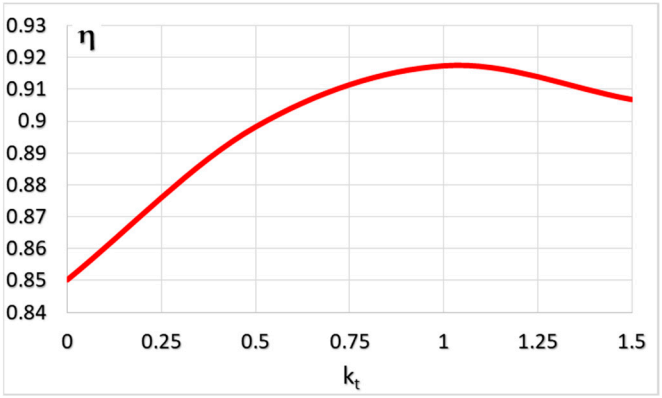


**Figure 6.** Variations of the planetary transmission efficiency, depending on $k_t$ (Case A).

(c) Rotor $R2$ is the most reactive to the variations of $k_\omega$ and $k_t$, which can change its state from the motor mode ($P_{R2} > 0$) to the brake mode ($P_{R2} < 0$) (Figures 3a and 4a); additionally, the power of rotor $R2$ is cancelled for $k_t = 1$, irrespective of the $k_\omega$ value.

(d) At normal operations ($k_\omega > 0$), rotor $R2$ works in the motor mode only for $k_t < 1$, becoming a brake for $k_t > 1$; for $k_\omega < 0$ (i.e., rotor $R2$ rotates in the same direction as the primary rotor $R1$), $R2$ becomes the motor only if $k_t > 1$ (see the line $k_\omega = -0.5$ in Figure 3a).

(e) Rotor $R3$ always operates in the motor mode ($P_{R3} > 0$), irrespective of the $k_t$ and $k_\omega$ values (Figures 3b and 4b); the power $P_{R3}$ increases linearly with the increase of $k_t$, while the slope of line $P_{R3}$ increases with $k_\omega$.

(f) The maximum power generated by rotor $R3$ ($P_{R3} = 6P_{R1}$ for $k_t = 1.5$ and $k_\omega = 1$, Figure 3b) is significantly higher than the maximum power of rotor $R2$ ($P_{R2} = P_{R1}$ for $k_t = 0$ and $k_\omega = 1$, Figure 3a).

(g) The mechanical power received by the generator increases linearly with the increase of the ratios $k_t$ and $k_\omega$ (Figure 5), even in the brake mode of rotor $R2$ ($P_{R2} < 0$ for $k_t > 1$ and $k_\omega > 0$, Figure 3a).

(h) The transmission efficiency does not depend on the ratio $k_\omega$ (see Table 3), but it is influenced by ratio $k_t$, with a maximum value of 0.917 for $k_t = 1$ (Figure 6), i.e., when the energy contribution of rotor $R2$ is zero ($P_{R2} = 0$, Figure 3a).

In conclusion, as $k_t$ and $k_\omega$ increase, the mechanical power supplied to the electric generator increases as well, with a higher input brought about by wind rotor $R3$ (Figures 3 and 4). The diagrams depicted in Figures 3–6 allow highlighting the particular cases in which the ratios $k_t$ and $k_\omega$ become null; by customization, the type A systems become types B ($k_\omega = 0$), C ($k_t = 0$) and D ($k_\omega = 0$, $k_t = 0$).

### *4.2. Power Flow*

In all four cases, the speed increaser contains a branched circuit of mechanical power, and the direction of the power flow in each branch depends on the $k_t$ and $k_\omega$ values; moreover, the three-rotor version (Case A) allows obtaining the other three cases by appropriate customizations: Case B ($\omega_{R2} = \omega_9 = \omega_{H_1} = 0$), Case C ($T_{R3} = T_8 = 0$) and Case D ($\omega_{R2} = \omega_9 = \omega_{H_1} = 0$ and $T_{R3} = T_8 = 0$).

The power flow is further analyzed comparatively, considering the input data from Table 4 and certain representative values $k_\omega \in \{0, 0.5, 1\}$ and $k_t \in \{0, 0.5, 1, 1.5\}$. According to Table 3, the powers in Case A depend on both the ratio $k_t$ and $k_\omega$; in Case B, only on $k_t$, and in Case C, only on $k_\omega$, while, in Case D, they are not influenced by these ratios.

- Case A

Six distinct simulation variants, defined by the distinct combinations of the $k_t$ and $k_\omega$ values, are addressed in Case A (see Figure 2a). The numerical results on the power flow are depicted in Figure 7, and the values of certain representative parameters are shown in Table 5. Based on the obtained data, the following aspects can be highlighted:

- The secondary rotors $R2$ and $R3$ influence each other when the pitch angle changes, their powers depending on both ratios $k_\omega$ (adjustment for $R2$) and $k_t$ (adjustment for $R3$).
- Ratio $k_t$ significantly influences both the power values and the directions of the power flows as follows:
  - $k_t = 0$: that is, Case C, in which the energetic contribution of rotor $R3$ is zero, such as $T_{R3} = 0$;
  - $0 < k_t < 1$ (red lines, Figure 7a,b): the powers of rotors $R1$, $R2$ and $R3$ flow branched and convergent towards the rotor and stator of the generator;

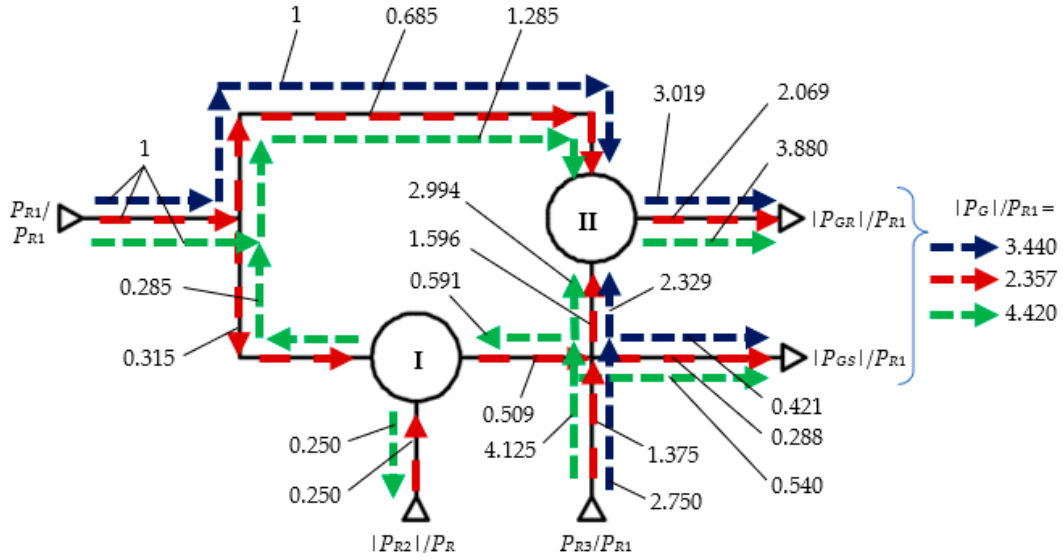


(a)

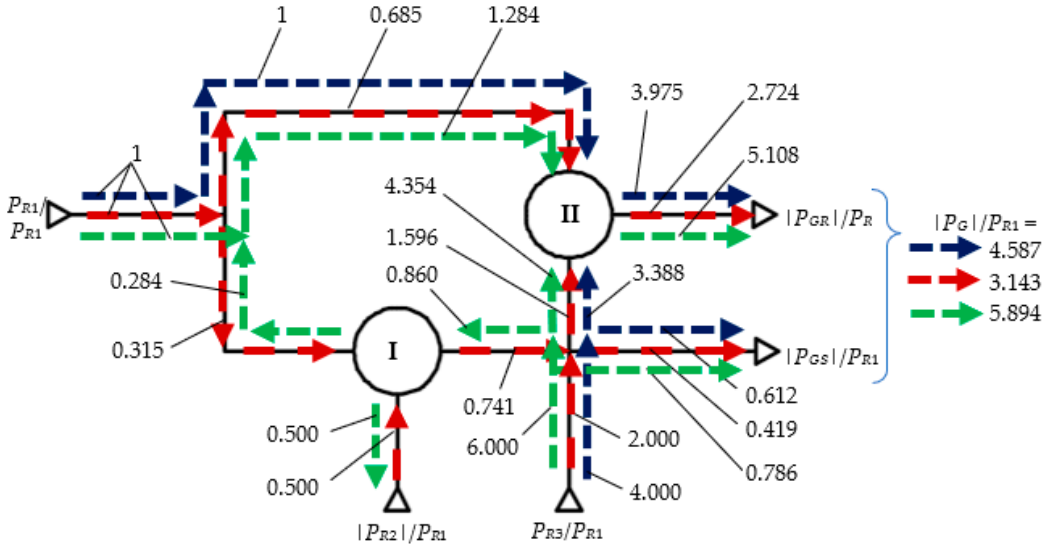


(b)

**Figure 7.** Reduced power flows of the 2-DOF and $L$ = 5 system (Case A) for: (**a**) $k_t = 0.5$ (red), 1 (blue), 1.5 (green) and $k_\omega = 0.5$; (**b**) $k_t = 0.5$ (red), 1 (blue), 1.5 (green) and $k_\omega = 1$.

- $k_t = 1$ (blue lines, Figure 7a,b): in this limit situation (when $T_{R2} = 0$ and $P_{R2} = 0$, see Tables 2 and 3), rotor *R*2 and the planetary gear set I are idling, and the power of rotor *R*1 flows through gear set II to *GR*, while the power of the rotor *R*3 branches into two flows: one directly to *GS* and another, through gear set II, to *GR*. It can be noticed that both the mechanical power of the generator and the transmission efficiency are higher compared with the previous situation ($0 < k_t < 1$);
- $k_t > 1$ (green lines, Figure 7a,b): the power flow of rotor *R*1 is transmitted entirely through gear set II to *GR*, while the power of rotor *R*3 branches into four streams: a first flow directly to *GS*, a second flow through gear set II to *GR*, a third flow through gear sets I and II also towards *GR* and a fourth flow through gear set I towards rotor *R*2, which passes in the brake mode, with the reversal of the power flow direction through planetary gear set I; although rotor *R*2 becomes the brake (reverse direction of $P_{R2}$ flow), the power received by the generator increases, while the transmission efficiency decreases (see Table 5).
  - The power $|P_G|$ received by the electric generator increases with the increase of the ratio $k_t$.
  - The power supply to the mobile stator *GS* increases with the increase of ratio $k_\omega$ (i.e., from 10% $P_G$ for $k_\omega = 0$ to 13.3% $P_G$ for $k_\omega = 1$).
  - The amplification ratio $i_a$ does not depend on ratio $k_t$ and increases with the increase of ratio $k_\omega$ (i.e., from 15 for $k_\omega = 0$ to 30 for $k_\omega = 1$, Table 5).
- Case B

Case B (Figure 2b) is derived from Case A by engaging clutch C1 (i.e., C1 = 1) and disengaging clutch C2 (i.e., C2 = 0 => $T_{R2} = 0$), accompanied by rotor *R*2 blocking ($\omega_{R2} = 0$ => $k_\omega = 0$). Comparing the best scenarios in Case A ($k_\omega = 1$ and $k_t = 1$) and in Case B ($k_t = 1$, see Table 5 and Figure 8): the rotor *R*3 power decreases about 2.66 times, the total input power and the output power decrease two times and the power input of the stator *GS* decreases to 10% of $P_G$.

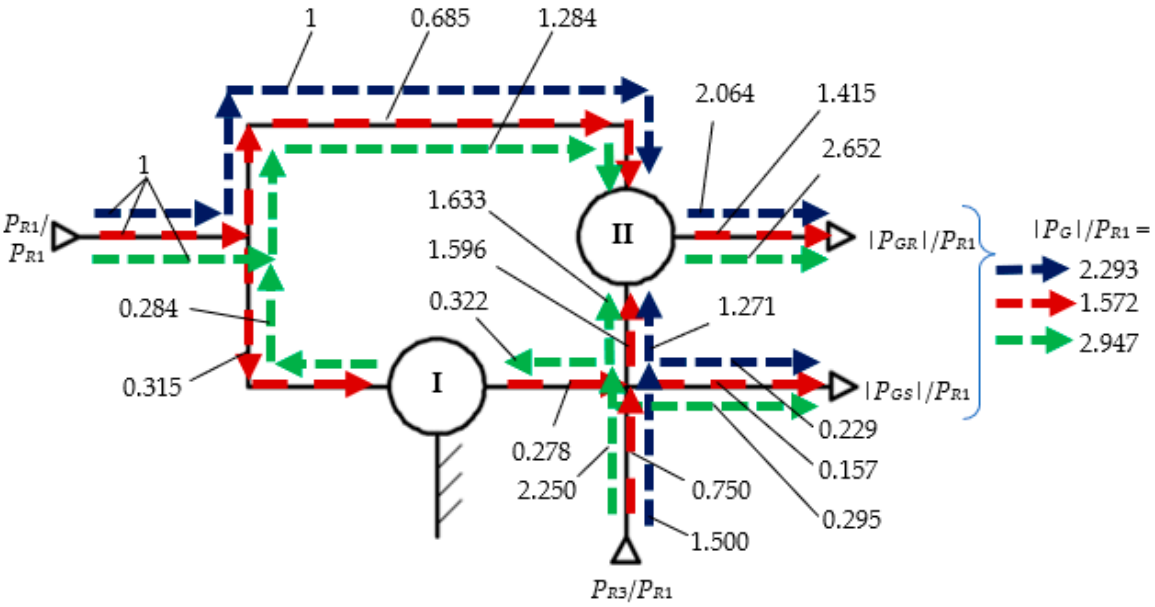


**Figure 8.** Reduced power flows of the 1-DOF and *L* = 4 system (Case B) for: $k_t = 0.5$ (red), 1 (blue) and 1.5 (green).

- Case C

Case C (Figure 2c) is obtained from Case A by eliminating rotor *R*3 ($T_{R3} = 0$ => $k_t = 0$) and the flows related to it; according to Figure 9, the flow corresponding to the value $k_\omega = 0$ is missing, because in this situation, Case C turns into Case D.

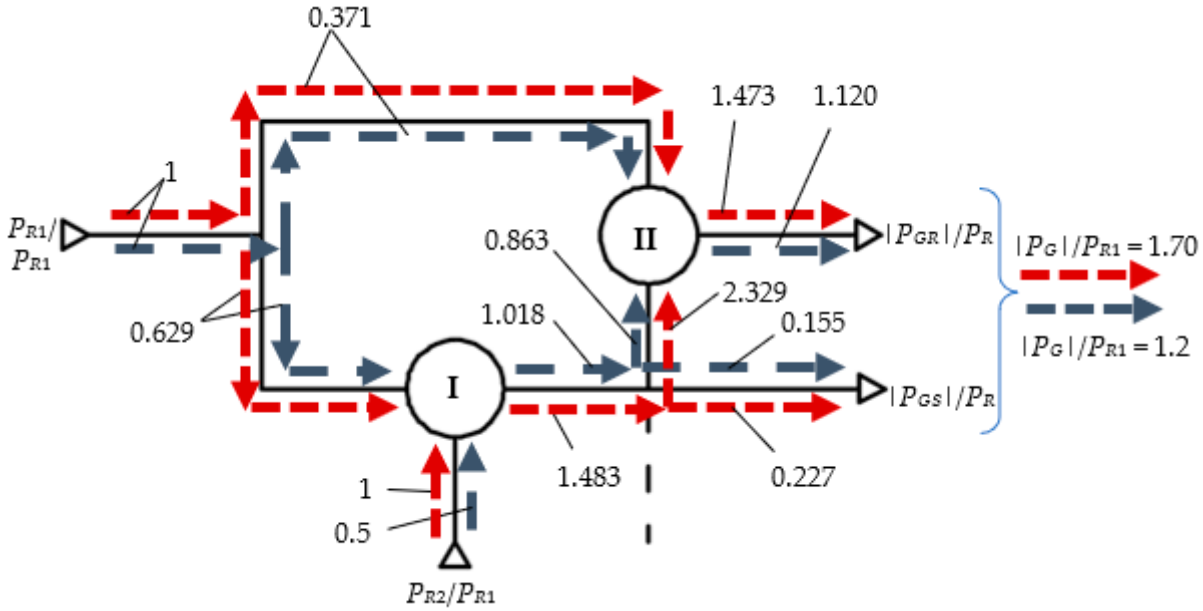


**Figure 9.** Reduced power flows of the 2-DOF and $L$ = 4 system (Case C) for $k_\omega = 0.5$ (blue) and 1 (red).

**Table 5.** Performances of the four *WSCGs* for certain representative numerical scenarios.

| Case | DOF | No WRs | $k_t$ | $k_\omega$ | $i_a$ | $P_{R2}/P_{R1}$ | $P_{R3}/P_{R1}$ | $P_{in}/P_{R1}$ | $\lvert P_G \rvert/P_{R1}$ | η | $P_{GS}/P_G$ |
|---|---|---|---|---|---|---|---|---|---|---|---|
| A | 2 | 3 | 0.5 | 1 | 30 | 0.500 | 2.000 | 3.500 | 3.143 | 0.898 | 13.3% |
| | | | 1 | 1 | 30 | 0 | 4.000 | 5.000 | 4.587 | 0.917 | 13.3% |
| | | | 1 | 0.5 | 22.5 | 0 | 2.750 | 3.750 | 3.440 | 0.917 | 12.2% |
| B | 1 | 2 | 0.5 | 0 | 15 | 0 | 0.750 | 1.750 | 1.572 | 0.898 | 10.0% |
| | | | 1 | 0 | 15 | 0 | 1.500 | 2.500 | 2.293 | 0.917 | 10.0% |
| C | 2 | 2 | 0 | 0.5 | 22.5 | 0.500 | 0 | 1.500 | 1.275 | 0.850 | 12.2% |
| | | | 0 | 1 | 30 | 1.000 | 0 | 2.000 | 1.700 | 0.850 | 13.3% |
| D | 1 | 1 | 0 | 0 | 15 | 0 | 0 | 1.000 | 0.850 | 0.850 | 10.0% |

Since ratio $k_t$ intervenes in the relation of the torques, powers and transmission efficiency (see Tables 2 and 3), Case C ($k_t = 0$) is characterized by the following particularities (Figure 9 and Table 5):

- the torque of the rotor *R*2 is equal, in absolute value, to that of the primary rotor *R*1; as a result, the power generated by *R*2 increases with the increase of the $k_\omega$ ratio;
- the input powers ($P_{R1}$ and $P_{R2}$) flow into three branches directly toward the rotor *GR* and stator *GS*;
- the transmission efficiency is constant (η = 0.85), regardless of the value of the ratio $k_\omega$;
- the power supply to the stator *GS* increases with the increase of $k_\omega$: from 12.1% $P_G$ for $k_\omega = 0.5$ to 13.3% $P_G$ for $k_\omega = 1$.

• Case D

Case D (Figure 2d) is derived from Case A by removing rotors *R*2 and *R*3, i.e., $k_\omega = 0$, $k_t = 0$; rotor *R*1 delivers a power whose flow (Figure 10) is similar to the homologous flow from Case C (see Figure 9). The system ensures a power supply of the stator *GS* of 10% of $P_G$ and a constant efficiency (η = 0.85).

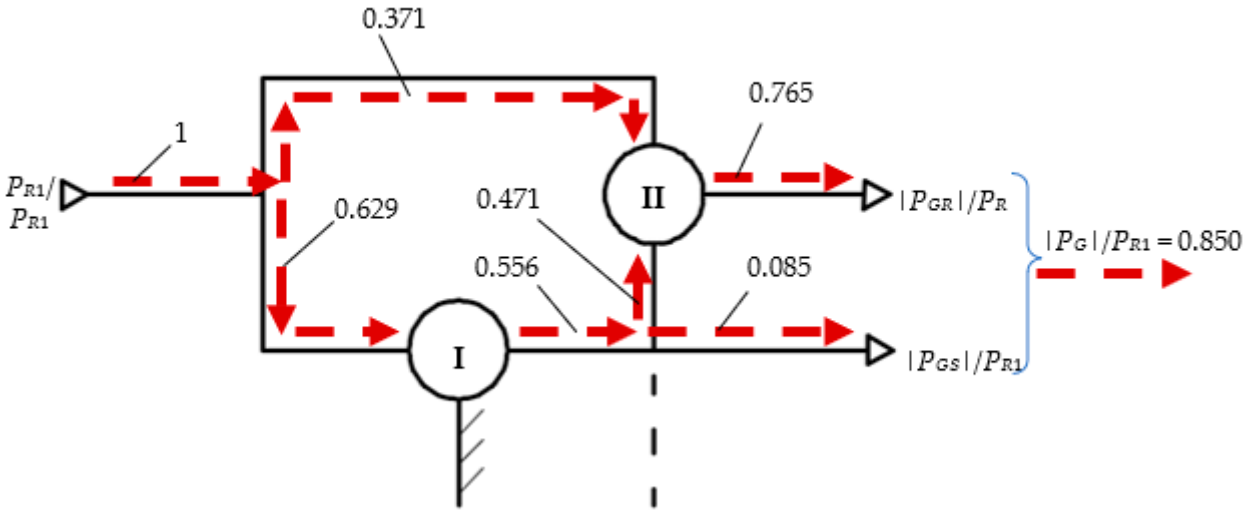


**Figure 10.** Reduced power flows of the 1-DOF and $L = 3$ system (Case D).

According to Table 5, both the structure's degree of freedom and the number of wind rotors have a major influence on the output power (to the generator) and on the input powers, as well as on the power distribution between secondary rotors *R*2 and *R*3, with a consistent increase for *R*3 in Case A. It should be noted that the 2-DOF transmissions double the speed amplification ratio ($i_a = 30$ for $k_\omega = 1$) compared to the 1-DOF ones ($i_a = 15$ for $k_\omega = 0$); a similar trend has the energy supply brought about by mobile stator *GS* (see the $P_{GS}/P_G$ ratio in Table 5). Being independent of the ratio $k_\omega$ and highly dependent on $k_t$, the transmission efficiency is higher in Cases A and B ($\eta = 0.917$, $k_t = 1$) vs. Cases C and D ($\eta = 0.850$, $k_t = 0$). The performances of the turbines with two wind rotors and 1-DOF (Case B) or 2-DOF (Case C) speed increasers significantly depend on $k_t$ and $k_\omega$; for the considered data, the 1-DOF transmission (Case B) shows a superior performance when $k_t = 1$ and $k_\omega = 1$.

## 5. Conclusions

This paper presented a comparative analysis of the performances of four different types of wind turbines with a counter-rotating electric generator. To this end, a differential planetary transmission with a variable structure, derived from an innovative solution proposed by the authors, was firstly proposed. By appropriate combinations of engaging/disengaging of the clutches, the transmission can operate in various structures, of which four cases were selected for analysis: a system with three rotors and a 2-DOF speed increaser (Case A), a 1-DOF system with two counter-rotating wind rotors (Case B), a 2-DOF system with two counter-rotating wind rotors (Case C) and 1-DOF system with a single wind rotor.

Archetype models for speeds, torques, powers and the efficiency of the planetary transmission with a variable structure used as speed increaser in the general case of differential transmission with three inputs (Case A) were developed. The analytical models of the other three cases (B, C and D) were the result of customizing the archetype models based on the correlations specific to each case according to the engaging/disengaging of the component clutches.

The analysis of the numerical results obtained by the simulations of the analytical models of the four *WSCGs*, considering a set of representative values for the simulation ratios $k_t$ and $k_\omega$, allowed drawing the following conclusions:

- the wind turbine with three wind rotors (Case A) allows the increase of the output powers (towards the electric generator) and of the input one compared to those with two counter-rotating wind rotors (Cases B and C); in turn, the systems in Cases B and

C can ensure a better use of the wind potential compared to traditional single-rotor wind turbines (Case D);

- the reduced input powers (corresponding to secondary wind rotors R2 and R3) and the reduced output power, as well as the configuration of the power flows, depend, to a large extent, on the values of ratios $k_t$ and $k_\omega$;
- the transmission efficiency is constant in Cases C and D, because it does not depend on the operating speed nor on the transmitted power; instead, the efficiency in Cases A and B changes with ratio $k_t$;
- thanks to the property of "summing up" the speeds, the 2-DOF systems (Cases A and C) can offer higher amplification ratios ($i_a$) than the 1-DOF ones and can implicitly ensure a higher power supply by the stator GS;
- the turbines with two wind rotors (Cases B and C) can have comparable power performances, the 1-DOF system (Case B) being advantaged with superior powers and efficiency in the vicinity of the value $k_t = 1$. The differential system (Case C) achieves higher amplification ratios, accompanied by relatively high powers, as the ratio $k_\omega$ increases;
- the maximum input power supply being brought about by rotor R3; the most interesting energy aspects are found in Case A in the vicinity of ratio value $k_t = 1$ for the situation $k_\omega = 0$. Practically, this means a 2-DOF system with two rotors, R1 and R3, were obtained from the case with three wind rotors by removing rotor R2 (i.e., Case B); it is also interesting that, in this system (Figure 1a without rotor R2), planetary gear set I idles (it does not participate in the transmission of the torque and of the power implicitly).

The authors intend to develop this topic more in the future by analyzing the CRWT behavior in dynamic conditions, the transient effects of changing the wind speed, by considering wind turbines and electric generators with known functional characteristics. The experimental validation of these theoretical results is also a future purpose of the authors.

**Author Contributions:** Conceptualization, M.N., R.S. and C.J.; methodology, M.N., R.S. and O.M.; software, R.S. and N.C.; validation, M.N., R.S., C.J. and O.M.; formal analysis, M.N., R.S., C.J. and O.M.; investigation, M.N., R.S., O.M. and N.C.; writing—original draft preparation, M.N., R.S, C.J. and O.M.; writing—review and editing, M.N., R.S., C.J., O.M. and N.C.; visualization, M.N., R.S., C.J., O.M. and N.C. and supervision, M.N. and C.J. All authors have read and agreed to the published version of the manuscript.

**Funding:** This research received no external funding.

**Institutional Review Board Statement:** Not applicable.

**Informed Consent Statement:** Not applicable.

**Data Availability Statement:** Not applicable.

**Conflicts of Interest:** The authors declare no conflict of interest.

## Nomenclature

Acronyms

| | |
|---|---|
| DOF | Degree of freedom |
| GR | Generator rotor |
| GS | Generator stator |
| WR | Wind rotor |
| WT | Wind turbine |
| WSCG | Wind system with counter-rotating generator |

| Symbols | |
|---|---|
| $C1,2,3$ | Clutch no 1, 2, 3 |
| $G$ | Electric generator |
| $H_{1,2}$ | Satellite carrier no 1, 2 |
| $i$ | Kinematic ratio ($i_{xy} = \omega_x/\omega_y$) |
| $i_0$ | Interior kinematic ratio |
| $\overline{i_0}$ | Interior static ratio |
| $i_a$ | Amplification kinematic ratio ($i_a = \omega_G/\omega_{R1}$) |
| I | Bevel planetary gear set |
| II | Spur planetary gear set |
| $k_t$ | Ratio of the input moments ($k_t = -T_{R3}/T_{R1}$) |
| $k_\omega$ | Ratio of the input angular speeds ($k_\omega = -\omega_{R2}/\omega_{R1}$) |
| $L$ | Total number of external links |
| $P$ | Power |
| $P_{in}$ | Sum on the input (positive) powers |
| $R1,2,3$ | Wind rotor no 1, 2, 3 |
| $T$ | Torque |
| $z$ | Gear teeth number |
| $\eta$ | Mechanical efficiency |
| $\eta_0$ | Internal mechanical efficiency |
| $\omega$ | Angular speed |

## References


1. Oprina, G.; Chihaia, R.A.; El-Leathey, L.A.; Nicolaie, S.; Babutanu, C.A.; Voina, A. A review on counter-rotating wind turbines development. *J. Sustain. Energy* **2016**, *7*, 91–98.
2. Didane, D.H.; Rosly, N.; Zulkafli, M.F.; Shamsudin, S.S. Performance evaluation of a novel vertical axis wind turbine with coaxial contra-rotating concept. *Renew. Energy* **2018**, *115*, 353–361. [CrossRef]
3. Pacholczyk, M.; Karkosinski, D. Parametric Study on a Performance of a Small Counter-Rotating Wind Turbine. *Energies* **2020**, *13*, 3880. [CrossRef]
4. West, R. Wind Turbine System. U.S. Patent 10,316,820 B2, 11 June 2019.
5. Neagoe, M.; Saulescu, R.; Jaliu, C. Design and Simulation of a 1 DOF Planetary Speed Increaser for Counter-Rotating Wind Turbines with Counter-Rotating Electric Generators. *Energies* **2019**, *12*, 1754. [CrossRef]
6. Saulescu, R.; Neagoe, M.; Jaliu, C. Conceptual Synthesis of Speed Increasers for Wind Turbine Conversion Systems. *Energies* **2018**, *11*, 2257. [CrossRef]
7. Mirnikjoo, S.; Abbaszadeh, K.; Abdollahi, S.E. Multi-Objective Design Optimization of a Double-Sided Flux Switching Permanent Magnet Generator for Counter-Rotating Wind Turbine Applications. *IEEE Trans. Ind. Electron.* **2020**, *68*, 6640–6649. [CrossRef]
8. Kutt, F.; Blecharz, K.; Karkosinski, D. Axial-Flux Permanent-Magnet Dual-Rotor Generator for a Counter-Rotating Wind Turbine. *Energies* **2020**, *13*, 2833. [CrossRef]
9. Neagoe, M.; Saulescu, R.; Jaliu, C.; Cretescu, N. Novel Speed increaser used in counter-rotating wind turbines. In *New Advances in Mechanisms, Mechanical Transmissions and Robotics*; Mechanisms and Machine Science Series; Springer: Berlin, Germany, 2017; Volume 46, pp. 143–151. [CrossRef]
10. Giger, U.; Kleinhansl, S.; Schulte, H. Design Study of Multi-Rotor and Multi-Generator Wind Turbine with Lattice Tower—A Mechatronic Approach. *Appl. Sci.* **2021**, *11*, 11043. [CrossRef]
11. Cho, W.; Lee, K.; Choy, I.; Back, J. Development and experimental verification of counter-rotating dual rotor/dual generator wind turbine: Generating, yawing and furling. *Renew. Energy* **2017**, *114*, 644–654. [CrossRef]
12. Jelaska, D.; Podrug, S.; Perkušic, M. A novel hybrid transmission for variable speed wind turbines. *Renew. Energy* **2015**, *83*, 78–84. [CrossRef]
13. Qiu, J.; Liu, B.; Dong, H.; Wang, D. Type Synthesis of Gear-box in Wind Turbine. *Procedia Comput. Sci.* **2017**, *109*, 809–816. [CrossRef]
14. Saulescu, R.; Jaliu, C.; Munteanu, O.; Climescu, O. Planetary Gear for Counter-Rotating Wind Turbines. *Appl. Mech. Mater.* **2014**, *658*, 135–140. [CrossRef]
15. Saulescu, R.; Jaliu, C.; Climescu, O.; Diaconescu, D. On the use of 2 DOF planetary gears as "speed increaser" in small hydros and wind turbines. In Proceedings of the ASME International Design Engineering Technical Conferences & Computers and Information in Engineering Conference IDETC/CIE 2011, Washington, DC, USA, 25–31 August 2011; pp. 601–610. [CrossRef]
16. Vasel-Be-Hagh, A.; Archer, C.L. Wind farms with counter-rotating wind turbines. *Sustain. Energy Technol. Assess.* **2017**, *24*, 19–30. [CrossRef]
17. Blanco, J.; Rodriguez, J.D.; Couce, A.; Lamas, M.I. Proposal of a Nature-Inspired Shape for a Vertical Axis Wind Turbine and Comparison of Its Performance with a Semicircular Blade Profile. *Appl. Sci.* **2021**, *11*, 6198. [CrossRef]
18. Pfaffel, S.; Faulstich, S.; Rohrig, K. Performance and Reliability of Wind Turbines: A Review. *Energies* **2017**, *10*, 1904. [CrossRef]

19. Fan, G.-F.; Qing, S.; Wang, H.; Hong, W.-C.; Li, H.-J. Support Vector Regression Model Based on Empirical Mode Decomposition and Auto Regression for Electric Load Forecasting. *Energies* **2013**, *6*, 1887–1901. [CrossRef]
20. Hong, W.C.; Fan, G.F. Hybrid Empirical Mode Decomposition with Support Vector Regression Model for Short Term Load Forecasting. *Energies* **2019**, *12*, 1093. [CrossRef]
21. Zhiqiang, L.; Yunke, W.; Jie, H.; Zhihong, Z.; Wenqi, C. The study on performance and aerodynamics of micro counter-rotating HAWT. *Energy* **2018**, *161*, 939–954. [CrossRef]
22. Lam, H.F.; Peng, H.Y. Measurements of the wake characteristics of co- and counter-rotating twin H-rotor vertical axis wind turbines. *Energy* **2017**, *131*, 13–26. [CrossRef]
23. Lipian, M.; Dobrev, I.; Massouh, F.; Jozwik, K. Small wind turbine augmentation: Numerical investigations of shrouded- and twin-rotor wind turbines. *Energy* **2020**, *201*, 117588. [CrossRef]
24. Bani-Hani, E.; Sedaghat, A.; Saleh, A.; Ghulom, A.; Al-Rahmani, H.; Al-Zamel, S.; Lopez, J. Evaluating Performance of Horizontal Axis Double Rotor Wind Turbines. *Energy Eng.* **2019**, *116*, 26–40. [CrossRef]
25. Erturk, E.; Sivrioglu, S.; Bolat, F. Analysis Model of a Small Scale Counter-Rotating Dual Rotor Wind Turbine with Double Rotational Generator Armature. *Int. J. Renew. Energy Res.* **2018**, *8*, 1849–1858. [CrossRef]
26. Pamuji, D.; Bramantya, M. Numerical Study on the Performance of 2-Bladed and 3-Bladed Counter Rotating Wind Turbines. *J. Jpn. Soc. Appl. Electromagn. Mech.* **2019**, *27*, 169–174. [CrossRef]
27. Neagoe, M.; Jaliu, C.; Saulescu, R.; Simionescu, P. Steady-State Response of a Dual-Rotor Wind Turbine with Counter-Rotating Electric Generator and Planetary Gear Increaser. In Proceedings of the MSR 2020 USCToMM Symposium on Mechanical Systems and Robotics, Rapid City, SD, USA, 14–16 May 2020; pp. 106–115. [CrossRef]
28. Fan, Z.; Zhu, C.; Li, X.; Liang, C. The transmission characteristic for the improved wind turbine gearbox. *Energy Sci. Eng.* **2019**, *7*, 1368–1378. [CrossRef]
29. Chaichana, T.; Chaitep, S. Performance Evaluation of Co-Axis Counter-Rotation Wind Turbine. *Energy Procedia* **2015**, *79*, 149–156. [CrossRef]
30. Didane, D.H.; Kudam, D.; Zulkafli, M.F.; Mohd, S.; Batcha, M.F.M.; Khalid, A. Development and Performance Investigation of a Unique Dual-rotor Savonius-type Counter-rotating Wind Turbine. *Int. J. Integr. Eng.* **2021**, *13*, 89–98. [CrossRef]
31. Didane, D.H.; Rosly, N.; Zulkafli, M.F.; Shamsudin, S.S. Numerical investigation of a novel contra-rotating vertical axis wind turbine. *Sustain. Energy Technol. Assess.* **2019**, *31*, 43–53. [CrossRef]
32. Cao, Y.; Han, Z.; Zhou, D.; Lei, H. Aerodynamic Performance of Counter-Rotating Vertical Axis Wind Turbine. *J. Shanghai Jiaotong Univ. Sci.* **2021**, *55*, 141–148. [CrossRef]
33. Ilmunandar, A.M.; Bramantya, M.A. Experimental Study of Counter Rotating Wind Turbine (Full Scale, R = 1.5 M) with Single Generator Using Gearbox. *Int. J. Sci. Technol. Res.* **2019**, *8*, 346–351.
34. Koehuan, V.; Sugiyono, S.; Kamal, S. Investigation of Counter-Rotating Wind Turbine Performance using Computational Fluid Dynamics Simulation. *IOP Conf. Ser. Mater. Sci. Eng.* **2017**, *267*, 12034. [CrossRef]
35. Li, Q.; Maeda, T.; Kamada, Y.; Murata, J.; Furukawa, K.; Yamamoto, M. Effect of number of blades on aerodynamic forces on a straight-bladed Vertical Axis Wind Turbine. *Energy* **2015**, *90*, 784–795. [CrossRef]
36. Maleki Dastjerdi, S.; Gharali, K.; Al-Haq, A.; Nathwani, J. Application of Simultaneous Symmetric and Cambered Airfoils in Novel Vertical Axis Wind Turbines. *Appl. Sci.* **2021**, *11*, 8011. [CrossRef]
37. Mirnikjoo, S.; Asadi, F.; Abbasazdeh, K.; Abdollahi, S.E. Effect of Rotor Topology on the Performance of Counter-Rotating Double-Sided Flux Switching Permanent Magnet Generator. *IEEE Trans. Energy Convers.* **2021**, *37*, 65–74. [CrossRef]
38. Jaliu, C.; Diaconescu, D.V.; Neagoe, M.; Saulescu, R. Dynamic features of speed increasers from mechatronic wind and hydro systems. Part I: Structure kinematics. In Proceedings of the EUCOMES 2008—The 2nd European Conference on Mechanism Science, Cassino, Italy, 17–20 September 2008; pp. 351–359. [CrossRef]
39. Saulescu, R.; Neagoe, M.; Munteanu, O.; Cretescu, N. Performance analysis of a novel planetary speed increaser used in single-rotor wind turbines with counter-rotating electric generator. *IOP Conf. Ser. Mater. Sci. Eng.* **2016**, *147*, 012090. [CrossRef]
40. Saulescu, R.; Jaliu, C.; Neagoe, M. Structural and Kinematic Features of a 2 DOF Speed Increaser for Renewable Energy Systems. *Appl. Mech. Mater.* **2016**, *823*, 367–372. [CrossRef]
41. Herzog, R.; Schaffarczyk, A.P.; Wacinski, A.; Zürcher, O. Performance and stability of a counter–rotating windmill using a planetary gearing: Measurements and Simulation. In Proceedings of the European Wind Energy Conference & Exhibition, Warsaw, Poland, 20–23 April 2010; pp. 1–8.
42. Bharani, R.; Sivaprakasam, A. A Review Analysis on Performance and Classification of Wind Turbine Gearbox Technologies. *IETE J. Res.* **2020**, *66*, 1–15. [CrossRef]
43. Nejad, A.R.; Keller, J.; Guo, Y.; Sheng, S.; Polinder, H.; Watson, S.; Dong, J.; Qin, Z.; Ebrahimi, A.; Schelenz, R.; et al. Wind turbine drivetrains: State-of-the-art technologies and future development trends. *Wind. Energy Sci.* **2022**, *7*, 387–411. [CrossRef]
44. Concli, F.; Pierri, L.; Sbarufatti, C. A Model-Based SHM Strategy for Gears—Development of a Hybrid FEM-Analytical Approach to Investigate the Effects of Surface Fatigue on the Vibrational Spectra of a Back-to-Back Test Rig. *Appl. Sci.* **2021**, *11*, 2026. [CrossRef]
45. Concli, F. Tooth Root Bending Strength of Gears: Dimensional Effect for Small Gears Having a Module below 5 mm. *Appl. Sci.* **2021**, *11*, 2416. [CrossRef]

46. Wu, J.; Zhou, Y.; Jiang, W.; Chen, X. Time-Domain Dynamic Modeling and Analysis of Complex Heavy-Duty Gearbox Considering Floating Effect. *Appl. Sci.* **2021**, *11*, 6876. [CrossRef]
47. Lee, G.H.; Park, Y.J.; Nam, J.S.; Oh, J.Y.; Kim, J.G. Design of a Mechanical Power Circulation Test Rig for a Wind Turbine Gearbox. *Appl. Sci.* **2020**, *10*, 3240. [CrossRef]
48. Lin, A.D.; Hung, T.P.; Kuang, J.H.; Tsai, H.A. Power Flow Analysis on the Dual Input Transmission Mechanism of Small Wind Turbine Systems. *Appl. Sci.* **2020**, *10*, 7333. [CrossRef]
49. Climescu, O.; Jaliu, C.; Saulescu, R. Comparative Analysis of Horizontal Small Scale Wind Turbines for a Specific Application. In Proceedings of the 14th IFToMM World Congress, Taipei, Taiwan, 25–30 October 2015; pp. 545–550. [CrossRef]
50. Saulescu, R.; Neagoe, M.; Jaliu, C.; Munteanu, O. Comparative Analysis of Two Wind Turbines with Planetary Speed Increaser in Steady-State. *Appl. Mech. Mater.* **2016**, *823*, 355–360. [CrossRef]
51. Saulescu, R.; Neagoe, M.; Cretescu, N. Comparative analysis of two wind turbines with counter-rotating vs. fixed-stator electric generator. *IOP Conf. Ser. Mater. Sci. Eng.* **2020**, *997*, 012091. [CrossRef]
52. Saulescu, R.; Neagoe, M.; Jaliu, C.; Munteanu, O. A Comparative Performance Analysis of Counter-Rotating Dual-Rotor Wind Turbines with Speed-Adding Increasers. *Energies* **2021**, *14*, 2594. [CrossRef]
53. Farahani, E.; Hosseinzadeh, N.; Ektesabi, M. Comparison of fault-ride-through capability of dual and single-rotor wind turbines. *Renew. Energy* **2012**, *48*, 473–481. [CrossRef]
54. Neagoe, M.; Saulescu, R.; Jaliu, C. Reconfigurable Wind System and Adjustment Method. Patent RO135228 (A0), 30 September 2021. *in press* (In Romanian).
55. Miloiu, G.; Dudita, F.; Diaconescu, D. *Modern Mechanical Transmissions*; "Tehnica" Publishing House: Bucharest, Romania, 1980. (In Romanian)